PCCP

ROYAL SOCIETY OF CHEMISTRY

PAPER

View Article Online
View Journal | View Issue

Cite this: *Phys. Chem. Chem. Phys.*, 2026, **28**, 4744

An efficient route to glyceraldehyde ($HOCH_2CH(OH)CHO$)—the simplest aldose—*via* reactions of carbon-centered radicals in deep space

Joshua H. Marks,†[ab] Jia Wang,†[ab] Ryan C. Fortenberry*[c] and Ralf I. Kaiser*[ab]

Received 14th November 2025,
Accepted 27th January 2026

DOI: 10.1039/d5cp04397b

rsc.li/pccp

The simplest sugar—glyceraldehyde ($HOCH_2CH(OH)CHO$)—represents a central molecule in the biochemistry of all lifeforms (glycolysis/gluconeogenesis). Linking photosynthesis and carbon fixation to sugar metabolism is fundamental to the liberation of energy from sugars and is the point at which glycolysis becomes exothermic—the pay-off phase. By exploiting isomer-selective photoionization reflectron time-of-flight mass spectrometry, glyceraldehyde and its energetic enol isomer 1,2,3-propenetriol ($HOCH_2C(OH)CHOH$) are identified *in situ* during space-simulation experiments as reaction products of radicals formed in ethylene glycol ($HOCH_2CH_2OH$) and carbon monoxide (CO) interstellar model ices exposed to energetic electrons as proxies for galactic cosmic rays. Isotopic substitution demonstrates the mechanism of sugar formation from molecules abundant in the interstellar medium. The stability of the carbon-centered radical intermediates formyl ($H\dot{C}O$) and 1,2-dihydroxyethyl ($HOCH_2\dot{C}HOH$) imply that reactions of carbon monoxide and methanol derivatives like ethylene glycol represent a facile, highly active mechanism of sugar production within ice coated interstellar grains in deep space.

Introduction

Little is known about the earliest life forms from which all modern life is descended other than it likely possessed traits common with the three modern domains of single-celled life: bacteria, archaea, and eukaryota.[1] Foremost among these shared characteristics are cellular encapsulation, genetics, and metabolism—all processes that require sugars and their derivatives (Fig. 1A).[2] Glycerol, a C3 sugar alcohol, represents the core component of the glycerophospholipids that comprise cell membranes. Additionally, ribose, a C5 aldose, and its derivative, deoxyribose, along with phosphate form the respective backbones of ribonucleic acid (RNA) and deoxyribonucleic acid (DNA).[3] Sugars are therefore central building blocks, energy source, and metabolites for all contemporary life. As the simplest sugars, glyceraldehyde (**1**) and its tautomer dihydroxyacetone (**4**) may have been an easily accessible food source and building-block for the first lifeforms (Fig. 1B).[4] Its adoption as one of the earliest energy sources is suggested by its position at the beginning of the 'pay-off phase' of glycolysis, *i.e.*, glucose is converted into two units of the glyceraldehyde-3-phosphate (**1**-PO_3^{2-}) by endoergic reactions which consume two molecules of adenosine triphosphate (ATP). During these reactions, **4**-PO_3^{2-} is rapidly formed and tautomerized into **1**-PO_3^{2-}. The exoergic decomposition of these two molecules of **1**-PO_3^{2-} is the portion of glycolysis from which energetic molecules like ATP and nicotinamide adenine dinucleotide phosphate (NADPH) are derived.[4] This sugar is produced during photosynthesis through the Calvin–Benson–Bassham cycle and is the starting point for biosynthesis of more complex sugars and sugar polymers such as starches.

Furthermore, glyceraldehyde (**1**) is a necessary material for the metabolic production of tryptophan (proteinogenic amino acid) and thiamine (vitamin B1).[5] Its central role in primitive biology is supported by the production of **1**-PO_3^{2-} in recent observations of non-enzymatic metabolism,[6,7] a system of biochemical reaction pathways that run parallel to glycolysis, the *S*-adenosylmethionine pathway, the Krebs cycle, and CO_2 fixation.[7] These reactions are implicated in the metabolism first explanation for the origins of life, where abundant ions (Fe^{2+}, Ca^{2+}) have been identified to catalyze many biochemical reactions under conditions relevant to the early Earth.[8–10] However, this explanation for the beginning of life requires the presence of a complex chemical environment in which

[a] *W. M. Keck Research Laboratory in Astrochemistry, University of Hawai'i at Manoa, Honolulu, Hawaii 96822, USA. E-mail: ralfk@hawaii.edu*
[b] *Department of Chemistry, University of Hawai'i at Manoa, Honolulu, HI 96822, USA*
[c] *Department of Chemistry & Biochemistry, University of Mississippi, Oxford, MS 38677, USA. E-mail: r410@olemiss.edu*
† These authors contributed equally to this work.

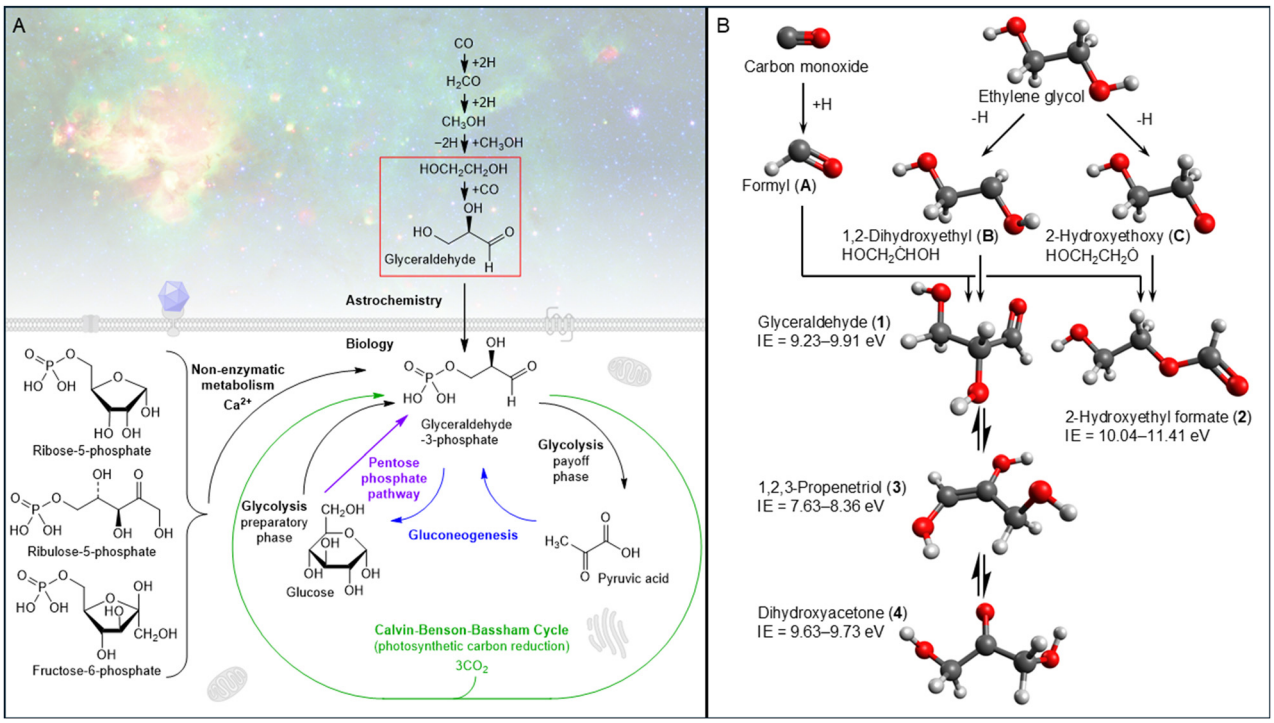

Fig. 1 (A) Reactions of key interstellar ice components (CO, H_2CO, CH_3OH) can efficiently produce glyceraldehyde (**1**) and the ubiquitous nature of this species in metabolism pointing to its early adoption during the development of life. (B) Interaction of ionizing radiation of ethylene glycol ($HOCH_2CH_2OH$) and carbon monoxide (CO) in interstellar model ices lead to formyl (**A**), 1,2-dihydroxyethyl (**B**), and 2-hydroxyethoxy radicals (**C**) undergoing radical–radical recombination to glyceraldehyde (**1**) and 2-hydroxyethyl formate (**2**); adiabatic ionization energies (IEs) of key products are calculated at the CCSD(T)-F12b/cc-pVTZ-F12b//B3LYP/aug-cc-pVTZ level of theory and include all possible conformers.

reagents and catalysts for these reactions are already present under often very specific reactant concentrations and conditions (pH, temperatures).[11–13]

The identification of sugars like glyceraldehyde (**1**) and dihydroxyacetone (**4**) in carbonaceous chondrite meteorites such as Murchison and Murray[14] affords strong evidence of exogeneous formation and delivery of complex biorelevant organics such as sugars, and in particular glyceraldehyde (**1**), to early Earth.[15] Here, we provide compelling evidence that glyceraldehyde (**1**) can likely be readily produced in the interstellar medium (ISM) on ice-coated nanoscale interstellar grains under the interstellar conditions found inside dense molecular clouds from which the Solar system is thought to have formed.[16] Exploiting isomer-selective photoionization reflectron time-of-flight mass spectrometry (PI-ReToF-MS) detection, the aldose glyceraldehyde (**1**) and its ketose tautomer dihydroxyacetone (**4**) are identified *in situ* during space-simulation experiments as the reaction products of radicals formed in ethylene glycol ($HOCH_2CH_2OH$) and carbon monoxide (CO) interstellar model ices exposed to proxies for galactic cosmic rays. The stability of the carbon-centered radical intermediates—the formyl radical (HĊO; **A**) and the 1,2-dihydroxyethyl radical ($HOCH_2\dot{C}HOH$; **B**)—imply that reactions of carbon monoxide and methanol derivatives like ethylene glycol may represent a facile, highly active mechanism of sugar production within ice coated interstellar nanoparticles in deep space. Both carbon monoxide[17–19] and methanol[20] are well known in the ISM. As an example, recent investigations by the James Webb Space Telescope targeting the nearby Chameleon cloud complex found that the pristine ice of the Chameleon I star-forming region contains carbon monoxide with a fractional abundance of up to 40% with respect to water.[21] Methanol (CH_3OH), a precursor to ethylene glycol ($HOCH_2CH_2OH$),[22,23] was also identified with 10% abundance relative to water.[21] Ethylene glycol have been detected, in molecular clouds composed of ice-coated nanoparticle-sized grains where the non-equilibrium chemistry demonstrated in such environments can take place.[24,25] Star-forming regions like the Orion KL nebula or the dense core Sgr B2(N-LMH) are host to the majority of astronomical detections of interstellar complex organic molecules, and both the Sagittarius[24] and Orion[25] molecular clouds are known to hold gas-phase ethylene glycol. Therefore, glyceraldehyde (**1**) may easily form in interstellar ice composed of carbon monoxide and methanol or ethylene glycol. Once synthesized, this sugar can be incorporated into planetesimals and may have eventually been delivered to planets such as early Earth through meteoritic and cometary impacts,[26–31] providing an exogenous source for the formation of essential biorelevant molecules, not only on Earth, but also in extra-solar planetary systems thus helping to decipher the enigma of the molecular origins of life in our Universe.

Experimental and computational

The experiments were conducted at the W. M. Keck Research Laboratory in Astrochemistry.[32–34] The apparatus is housed in a

hydrocarbon-free stainless steel ultra-high vacuum (UHV) chamber which is maintained at a few 10^{-11} Torr by magnetically levitated turbomolecular pumps.[35] A closed cycle helium refrigerator (Sumitomo Heavy Industries, RDK-415E) cools a mirror-polished silver wafer (15.1 × 12.6 mm for PI-ReToF-MS) to 5.0 ± 0.2 K. The cryostat-wafer assembly is rotatable about the vertical axis because it is mounted on a doubly differentially pumped rotatable flange (Thermionics Vacuum Products, RNN-600/FA/MCO), and can be translated along its rotation axis *via* an adjustable bellows (McAllister, BLT106). Ices were prepared by passing CO (Matheson, 99.99%; ^{13}CO Sigma Aldrich, 98% atom ^{13}C; C^{18}O, Sigma Aldrich, 99% atom ^{18}O) and ethylene glycol ($HOCH_2CH_2OH$, Sigma Aldrich, 99.8%; $HO^{13}CH_2CH_2OH$, Sigma Aldrich, 99% atom ^{13}C) through separate 10 mm diameter glass capillary arrays directed at the cooled wafer. Partial pressures of each ice component were adjusted using leak valves to achieve approximately a 3 : 1 ratio of [ethylene glycol] : [carbon monoxide]. This ratio was chosen to obtain the highest possible yield of $C_3H_6O_3$ isomers and thereby facilitates their detection. The ice thickness was determined by monitoring the ice deposition with a helium-neon laser (CVI Melles-Griot, 25-LHP-230, 632.8 nm) at a 2° angle of incidence and measuring variations in reflected power due to thin film interference by the ice.[36] The index of refraction was determined by the average of the indexes of refraction of the two components, 1.25 ± 0.03 for carbon monoxide[37] and 1.46 ± 0.05 for ethylene glycol with an average of 1.36 ± 0.06. Details of the composition and thickness of ices studied are reported in Table S1. After deposition at 5 K, the ice mixtures were irradiated with 5 keV energetic electrons (SPECS, EQ PU-22) at an incidence angle of 70° with a current of 30 nA for 60 minutes. 5 keV electrons were employed because their linear energy transfer is comparable to that of 10–20 MeV GCR protons deposited in interstellar ices.[38,39] The effective doses reported here are the result of simulating the trajectories of an ensemble of electrons using CASINO 2.42 (Table S2). The average penetration depth of the electrons is then used to determine the volume of irradiated ice and therefore the average dose, in place of the ice thickness determined through interferometry.

Fourier transform infrared (FTIR) spectra (Thermo Electron, Nicolet 6700) were collected in the range 6000–500 cm^{-1} with 220 spectra averaged over a two-minute period after ice deposition and used to calculate the relative abundance of the two components (Fig. S1 and S2). Relative concentrations of ethylene glycol and carbon monoxide in ices were determined using integrated infrared absorption strength of the components. For carbon monoxide, the narrow and strong absorption due to ^{12}CO stretching at 2139 cm^{-1} saturates the detector, instead the same absorption of ^{13}CO at 2092 cm^{-1} with a known absorption coefficient of 1.32×10^{-17} cm molecules^{-1}. For ethylene glycol, the absorption coefficients were determined by depositing 480 nm of ethylene glycol, deconvoluting its FTIR spectrum, and calculating the ratio of intensity to number of molecules (Fig. S1, S3 and Table S3).

The photoionization reflectron time-of-flight mass spectrometry (PI-ReToF-MS) technique has been discussed in detail elsewhere.[33,40] Ices were heated to 320 K with temperature programmed desorption (TPD) at a rate of 1 K min^{-1}. During TPD, pulsed 30 Hz coherent vacuum ultraviolet (VUV) light was passed 1–2 mm above the surface of the ice to photoionize subliming molecules. VUV light was produced *via* resonant difference four-wave mixing ($\omega_{VUV} = 2\omega_1 - \omega_2$) schemes (Table S4). After generation of the selected ω_1 and ω_2, the lasers were aligned collinear and directed through a lens (Thorlabs, LA5479, f = 300 mm) and focused into a jet of rare gas in the VUV generation vacuum chamber. Coherent VUV light exiting this chamber was separated from ω_1 and ω_2 by passing the collinear beams through an off-axis lithium fluoride (LiF) biconvex lens (Korth Kristalle, $R_1 = R_2$ = 131.22 mm) which imparts an angular separation between the three frequencies and directs only the VUV light through an aperture to the ionization region. Ions formed are mass-analyzed in a reflectron time-of-flight mass spectrometer (ReToF-MS; Jordan TOF Products) and detected with a dual microchannel plate (MCP) detector in the chevron configuration (Jordan TOF Products). MCP signal was amplified (Ortec, 9305) before discrimination and amplification to 4 V (Advanced Research Instruments Corp., F100-TD) and recorded by a multichannel scaler (FAST ComTec, MCS6A). Ion arrival times were recorded to 3.2 ns accuracy; mass spectra were accumulated every two minutes during TPD.

The adiabatic ionization energies (IEs) and relative energies (ΔE) are computed as zero-point vibrational energy (ZPVE) corrected adiabatic differences in the energies of the neutral and radical–cation geometries (Table S5). B3LYP/aug-cc-pVTZ is used to optimize the geometries and compute the harmonic vibrational energies in Gaussian16 (Tables S6–S9).[41–45] Explicitly correlated coupled-cluster singles, doubles, and perturbative triples (CCSD(T)-F12b) employing the cc-pVTZ-F12 basis set as available within MOLPRO 2020[46–50] produces the single-point energies at the optimized B3LYP/aug-cc-pVTZ geometries, denoted as CCSD(T)-F12b/cc-pVTZ-F12b//B3LYP/aug-cc-pVTZ. These CCSD(T)-F12b energies along with the B3LYP-derived ZPVEs produce IE and ΔE. This approach has demonstrated excellent correlation with experiments in previous work with accuracies of the calculated adiabatic ionization energies of ±0.05 eV.[51]

Results

Fourier transform infrared spectroscopy (FTIR)

Infrared spectroscopy is an invaluable tool for identifying the depletion of reactants and the presence of sufficiently abundant product functional groups and small molecules. Respective doses of 5.6 ± 0.6 eV molecule^{-1} for ethylene glycol and 2.6 ± 0.3 eV molecule^{-1} for carbon monoxide are imparted during irradiation constituting 2–10% of the dose expected over the lifetime of an interstellar molecular cloud.[52] While the absorption of the C≡O stretching mode at 2139 cm^{-1} is strong enough to saturate the detector, the sharp and isolated absorption of ^{13}CO at 2090 cm^{-1} demonstrates a 10% reduction in intensity (Fig. 2) showing its consumption by reactions in the ice during irradiation. New absorbance bands in the carbonyl

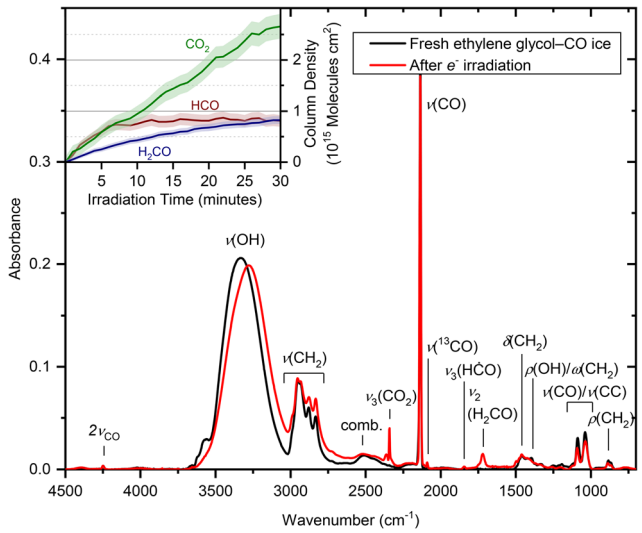

Fig. 2 Fourier transform infrared (FTIR) spectra of ethylene glycol–carbon monoxide ice when freshly deposited (black) and after electron irradiation (red) with a dose of 5.6 ± 0.6 eV molecule^{-1} for ethylene glycol and 2.6 ± 0.3 eV molecule^{-1} for carbon monoxide. This represents an energetic dose equivalent of up to 10% of that experienced by ices contained in interstellar molecular clouds over its lifetime.

(C═O) stretching region of 1850–1550 cm^{-1} are easy to detect because of the otherwise flat baseline.[53] These peaks (Fig. 2, inset) can be attributed to the rapid formation of carbon dioxide (CO_2; ν_3, 2342 cm^{-1}) and formaldehyde (H_2CO; ν_2, 1718 cm^{-1}) by respective oxidation and reduction of CO. Critically, an intermediate in the proposed reaction scheme (Fig. 1B), the formyl radical (**A**) is observed here by its carbonyl stretching mode (ν_2, 1844 cm^{-1}). Further changes to the infrared spectrum speak to the diversity of new molecules containing hydroxyl (–OH) or hydrocarbon (–CH) moieties. The broad peak 3600–3000 cm^{-1} can be linked to the hydrogen-bonded hydroxyl stretches of ethylene glycol and the set of four smaller peaks in the 3000–2700 cm^{-1} range are produced by its four CH stretching modes.[54] These peaks undergo substantial broadening and redshift due to the presence of a diverse range of chemical environments and product molecules containing these moieties generated during irradiation. The presence of formyl as an aldehyde precursor is crucial evidence for the reaction mechanism proposed in Fig. 1A. Recombination of this radical with the 1,2-dihydroxyethyl radical (**B**) produced by Ḣ loss from ethylene glycol during irradiation is a one-step radical recombination route to glyceraldehyde. The infrared absorptions of **B**, 2-hydroxyethoxy ($HOCH_2CH_2\dot{O}$; **C**), and glyceraldehyde broadly overlap with those of the reactants and other products, and without a distinct feature like that of **A**, identifying the presence of this sugar demands more sensitive techniques.

Photoionization reflectron time-of-flight mass spectrometry (PI-ReToF-MS)

Ices studied are subjected to the temperature, pressure, and irradiation conditions found within an interstellar cloud prior to its gravitational collapse and star formation. This later stage of the molecular cloud lifecycle is simulated through the slow heating of the sample, which also induces sublimation of the ice in temperature-programmed desorption (TPD) at a rate of 0.5 K min^{-1}. During this procedure, coherent vacuum ultraviolet light (VUV) photoionizes subliming molecules for mass analysis. Experiments were conducted using photoionization at 10.49, 9.98, 9.13, and 7.45 eV (Fig. 3). Variations in adiabatic ionization energies among glyceraldehyde and its isomers (Fig. 1) are exploited to provide evidence on the identification of the molecules produced and desorbed during these space simulation experiments. The ionization energies used in the identification of these species are calculated at the composite CCSD(T)-F12b/cc-pVTZ-F12b//B3LYP/aug-cc-pVTZ level of theory and are represented by ranges that include the adiabatic ionization energies of all conformational isomers within each structural isomers and an error of ±0.05 eV.[51,55,56]

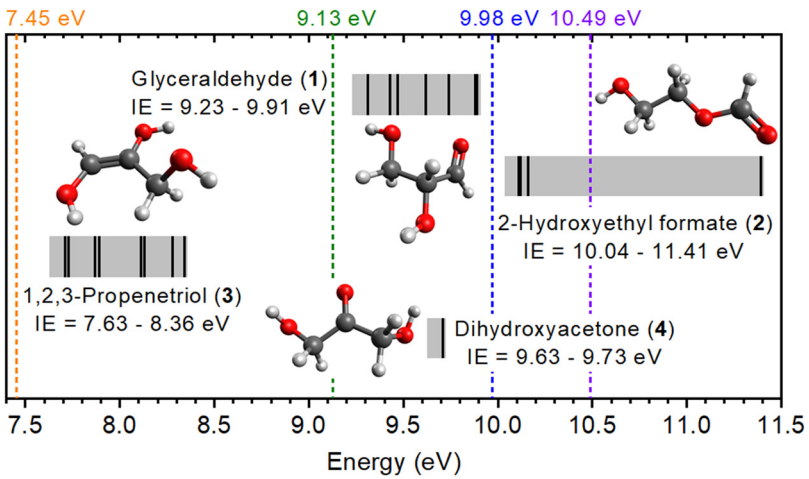

Fig. 3 Products of reactions within an ice can be identified by ionizing distinct structural isomers by accounting for their varying adiabatic ionization energies (IEs). The calculated IEs (black solid line) and their IE ranges (gray area) are shown, with combined uncertainty limits of −0.05/+0.05 eV and a correction of −0.03 eV applied to account for the thermal and Stark effects.

Photons with an energy of 10.49 eV can ionize all structural and conformational isomers of glyceraldehyde except for one conformer of 2-hydroxyethyl formate (**2a**) which is 27 kJ mol^{-1} less stable than the minimum energy conformer. In contrast, photoionization at 9.98 eV prevents detection of any conformer of 2-hydroxyethyl formate (**2**) while structural isomers glyceraldehyde (**1**), 1,2,3-propenetriol (**3**), and dihydroxyacetone (**4**) should be detectable if present. It is important to note that low dose electron irradiation was employed to minimize sequential reactions, thereby limiting the accessible formation pathways of $C_3H_6O_3$ isomers. Previous laboratory simulation experiments of irradiated interstellar ice analogues have demonstrated that the decomposition of the organic molecules is dictated by simple bond ruptures ejecting H atoms such as C–H,[57–66] N–H,[67–71] and O–H.[72–76] Under these low-temperature conditions, isomers **1–4** are proposed to form *via* radical–radical recombination, followed by tautomerization processes.[60,62] During experiments with 10.49 eV photoionization, three peaks are identified at 220, 250, and 280 K in the mass spectrum at m/z = 90 (Fig. 4A). The first of these peaks corresponds to the sublimation of ethylene glycol as evidenced in Fig. S4 by an intense central peak at 10.49 and 9.98 eV (Fig. S5) and may be attributed to the co-sublimation of reaction products weighing 90 amu or the fragmentation of a larger species co-subliming; this feature cannot be confidently attributed to any of the target molecules. Conversely, the peaks at 250 and 280 K do not correspond to another sublimation event like that of ethylene glycol. However, from their detection at 9.98 eV, neither the peak at 250 nor 280 K can clearly be attributed to 2-hydroxyethyl formate (**2**).

Where photoionization remains possible for glyceraldehyde (**1**, IE = 9.23–9.91 eV), 1,2,3-propenetriol (**3**, IE = 7.63–8.36 eV), and dihydroxyacetone (**4**, IE = 9.63–9.73 eV) with 9.98 eV photons, only 1,2,3-propenetriol (**3**) can be photoionized at 9.13 eV. During experiments employing 9.13 eV photons, only the peak at 250 K can be seen while the peak at 280 K is no longer detectable. This is strong evidence for glyceraldehyde (**1**) as the identity of the 280 K peak. While dihydroxyacetone (**4**) is likely also present, it cannot be distinguished from glyceraldehyde (**1**) based on photoionization energy (Fig. 3). Furthermore, the proposed route to dihydroxyacetone (**4**) (Fig. 1B) requires its production *via* tautomerization of glyceraldehyde (**1**). Tautomer 1,2,3-propenetriol (**3**) can be ionized with photons at 9.13 eV but cannot be ionized with photons at 7.45 eV. Experiments employing 7.45 eV photons for ionization do not detect this peak (Fig. 4D), and this peak can then be attributed to 1,2,3-propenetriol (**3**), while analysis of the molecular formula(e) is necessary for confirmation.

Isotopic substitution experiments employing ^{18}O and ^{13}C labelling were used to verify that the molecular formula of these identified peaks indeed correspond to $C_3H_6O_3$. During TPD of irradiated ethylene glycol–C^{18}O ices the three identified peaks at 220, 250, and 280 K can be deconvoluted from the resulting TPD profile using the same fitting functions by varying only their relative intensity (Fig. 5B). Note that the TPD profiles of the isotope-labelled experiments are not identical, as the absolute signal intensities can vary due to isotope-dependent reaction

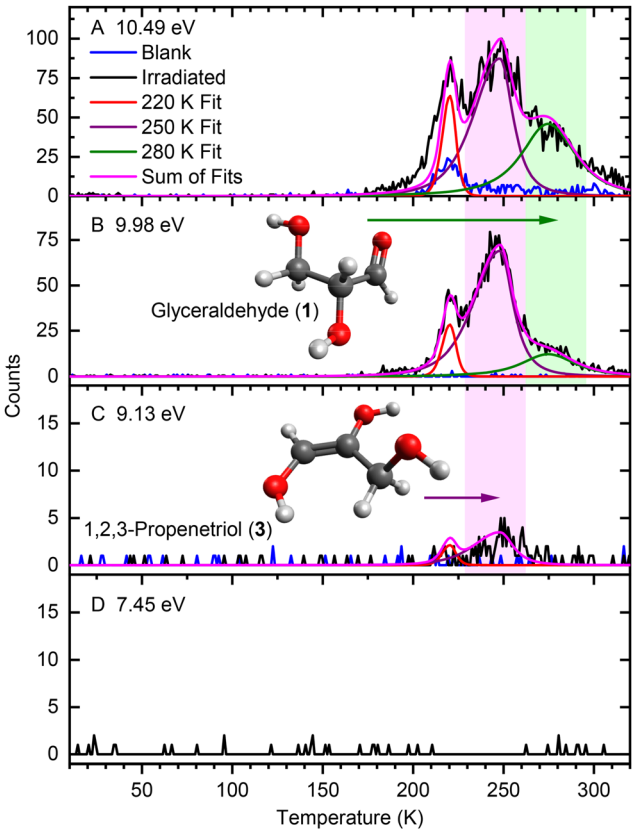

Fig. 4 PI-ReToF-MS mass spectra of blank (unirradiated, blue) and irradiated (black) ethylene glycol–carbon monoxide ices studied with photon energies of (A) 10.49, (B) 9.98, (C) 9.13, and (D) 7.45 eV. The peak at 220 K (red) is the result of reaction products that co-sublime with the ethylene glycol matrix and cannot be uniquely assigned to any molecule. The peak at 250 K (purple) can be linked to detection of 1,2,3-propenetriol (**3**) while the deconvoluted peaks at 280 K (green) are attributed to glyceraldehyde (**1**).

yields and detection efficiencies. Further confirmation of the molecular formula requires analysis of ethylene glycol–$^{13}C_2$–CO (Fig. 5C) and ethylene glycol–$^{13}C_2$–^{13}CO (Fig. 5D) ices. In these experiments the three peaks observed in prior experiments are readily identifiable and can be deconvoluted by only varying the intensity of the same fitting functions. No single species can be identified from the 220 K peak, the identification of the sublimation events at 250 and 280 K from ices containing ^{13}CO and C^{18}O with a respective isotopic mass shift of only 1 or 2 amu is a clear demonstration of the inclusion of only one molecule of CO reactions resulting in the 90 amu product. Furthermore, ethylene glycol–$^{13}C_2$ in combination with ^{13}CO resulted in an isotopic mass shift of 3 amu, indicating the inclusion of only one molecule of ethylene glycol in the 90 amu product. This is also supported by ethylene glycol–d_4–CO ice experiment in which the TPD profile of m/z = 93 recorded at 10.49 eV matches that of irradiated ethylene glycol–CO ice (Fig. S6). The remaining mass must then be accounted for entirely with H and O, thereby confirming that the formula must be $C_3H_6O_3$. Thus, the peaks identified earlier (Fig. 4) represent the detection of these molecules belonging to 1,2,3-propenetriol (**3**) at 250 K and glyceraldehyde (**1**) at 280 K.

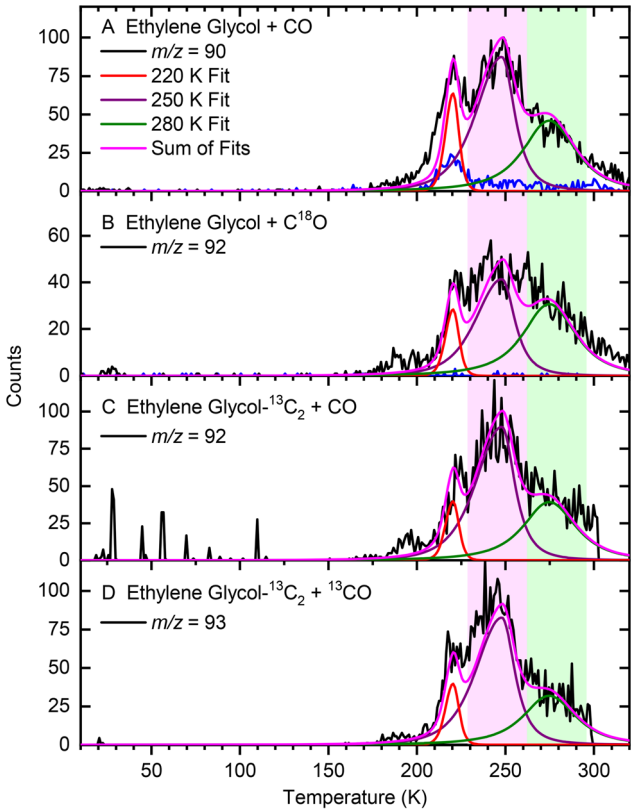

Fig. 5 PI-ReToF-MS mass spectra measured with 10.49 eV photons during TPD of irradiated ices composed of (A) ethylene glycol–carbon monoxide, (B) ethylene glycol–carbon monoxide–^{18}O, (C) ethylene glycol–$^{13}C_2$–carbon monoxide, and (D) ethylene glycol–$^{13}C_2$–carbon monoxide–^{13}C. The fitted functions (red, purple, and green) and their sum (magenta) are obtained by varying only the intensity of the same set of functions derived from experiments in which the photon energy was varied (Fig. 4).

Discussion

Formation of glyceraldehyde

The key finding resulting of these experiments is the identification of glyceraldehyde (**1**)—the simplest biologically active sugar—*in situ*, during space-simulation, with mechanistic details. The proposed reaction scheme (Fig. 1) requires an initial unimolecular dissociation of ethylene glycol in reactions (1a) and (1b) deposited in the ice prior and an addition of the suprathermal hydrogen radical (Ḣ) released in these processes to carbon monoxide forming the formyl radical (HĊO; **A**) in reaction (2).

$$HOCH_2CH_2OH + GCR \rightarrow HOCH_2\dot{C}HOH\ (\mathbf{B}) + \dot{H} \quad (1a)$$

$$HOCH_2CH_2OH + GCR \rightarrow HOCH_2CH_2\dot{O}\ (\mathbf{C}) + \dot{H} \quad (1b)$$

$$CO + \dot{H} \rightarrow H\dot{C}O\ (\mathbf{A}) \quad (2)$$

A small barrier to addition faced by reaction (2) has been experimentally measured to be 8 kJ mol^{-1} in the gas phase.[77–79] The temperatures at which the irradiation was conducted (5 K) prevent the possibility of this barrier being overcome through thermal energy, but rather the suprathermal kinetic energy is imparted to the hydrogen radical during dissociation of ethylene glycol in reactions (1a) and (1b) which allows it to overcome this barrier easily.[80] The production of radical **A** is readily identifiable in the studied ices through its unique Ċ═O stretching vibration (ν_3) at 1839 cm^{-1}. The absorption intensities of CO_2, H_2CO, and HĊO (Fig. 2, inset) increase in abundance throughout the irradiation. While CO_2 demonstrates a nearly linear relationship between irradiated dose and concentration, H_2CO and **A** are found to be highly non-linear, where the latter reaches steady-state concentration of 0.85 × 10^{15} molecules cm^{-2} after 8 minutes of irradiation and a total dose of 0.8 ± 0.3 eV molecule^{-1} for ethylene glycol. Observation of abundant intermediate **A** and its apparently non-linear increase in concentration with respect to dose is a key finding in the context of the proposed reaction scheme. Preliminary experiments employed only 0.5 ± 0.1 eV molecule^{-1} for ethylene glycol, but were unable to produce detectable quantities of any 90 amu product. The rate of reactions following the production of these radicals may be limited by a dependence on the concentration of **A**. This both explains the lack of glyceraldehyde (**1**) in the low-dose experiment and suggests the validity of the proposed radical reaction scheme.

Recombination of the radical intermediates faces no barrier, though radicals must achieve the proper orientation for radical–radical recombination reactions (3) and (4) to take place, *i.e.*, radical sites must face each other to recombine.[81,82]

$$H\dot{C}O\ (\mathbf{A}) + HOCH_2\dot{C}HOH\ (\mathbf{B}) \rightarrow HOCH_2CH(OH)CHO\ (\mathbf{1}) \quad (3)$$

$$H\dot{C}O\ (\mathbf{A}) + HOCH_2CH_2\dot{O}\ (\mathbf{C}) \rightarrow HOCH_2CH_2OCHO\ (\mathbf{2}) \quad (4)$$

These recombination reactions can only occur once irradiation has started to provide a source of the intermediates. Doubtless, due to extremely limited molecular rotation and diffusion at 5 K, some radicals are consumed by these and other recombination reactions as TPD begins and thermal energy permits molecular motion.

Sequential tautomerization reactions (5) and (6) may produce 1,2,3-propenetriol (**3**) and dihydroxyacetone (**4**).

$$HOCH_2CH(OH)CHO\ (\mathbf{1}) \leftrightarrow HOCH_2C(OH)CHOH\ (\mathbf{3})$$
$$\Delta_r H^\circ(0\ K) = 80\ kJ\ mol^{-1} \quad (5)$$

$$HOCH_2C(OH)CHOH\ (\mathbf{3}) \leftrightarrow HOCH_2COCH_2OH\ (\mathbf{4})$$
$$\Delta_r H^\circ(0\ K) = -59\ kJ\ mol^{-1} \quad (6)$$

While interconversion between glyceraldehyde (**1**) and dihydroxyacetone (**4**) is known in room-temperature aqueous solution, it is not clear that this is a plausible route in a solid at 5 K, especially without the assistance of a protic solvent like water. Unlike the reactions leading to glyceraldehyde (**1**), these tautomerization processes are not barrierless but are equilibrium-driven; their kinetics therefore depend on both the temperature and the local chemical environment and require prior formation of glyceraldehyde (**1**) at 5 K. One formulation of the Erlenmeyer rule states that a C═C bond adjacent to a hydroxyl group is inherently unstable.[83] Here this behavior is demonstrated in the instability of the enol 1,2,3-propenetriol (**3**) with

respect to both keto forms glyceraldehyde (**1**) and dihydroxyacetone (**4**), which are 59–80 kJ mol^{-1} more stable, based on minimum energy conformations. Formation of ethylene glycol may proceed with a single initiating event provided by GCR or energetic secondary electrons. However, proceeding toward tautomerization reactions (5) and (6) requires further initiation. Observation of 1,2,3-propenetriol (**3**) subliming at 250 K (Fig. 4) is evidence that these barriered reactions take place. Although dihydroxyacetone (**4**) shares the same molecular mass, ionization energy, functional groups, and likely a comparable sublimation temperature with glyceraldehyde (**1**), no direct evidence for the formation of dihydroxyacetone (**4**) can be obtained under the present experimental conditions.

Origin of glyceraldehyde's precursors

For glyceraldehyde (**1**) or dihydroxyacetone (**4**) to form, its precursors must first be available. For example, methanol (CH_3OH) is the fourth most abundant interstellar ice component and is thought to be produced in large quantities by GCR irradiation of ices containing water (H_2O) and CO.[84] It can reach abundances of 20% relative to water through hydrogenation of CO as clouds age and undergo energetic processing by GCRs.[21,85] CO itself is the second most abundant ice component after water and is present at up to 70% relative to water in star-forming regions.[21] Radical reactions of methanol have been proposed as a major route toward the formation of ethylene glycol in the interstellar medium. Reactions of suprathermal Ḣ with increasingly saturated CO-containing molecules in reactions (7) and (8), which build on reaction (2).

$$CO + 2\dot{H} \rightarrow H_2CO \quad (7)$$

$$H_2CO + 2\dot{H} \rightarrow CH_3OH \quad (8)$$

Formaldehyde (H_2CO) evolved during irradiation by reaction (7) is readily detectable (Fig. 2 inset), but (8) produces methanol (CH_3OH) which only contains moieties already present in ethylene glycol and cannot be selectively detected here. For similar reasons, the abundance of methanol in the ISM prevents firm identification of ethylene glycol in ices, however abundant it has been found to be in the gas phase. Production of ethylene glycol itself in reaction (9) is efficient in comparison to competing dimerization reactions that produce methoxymethanol (CH_3OCH_2OH) and dimethyl peroxide (CH_3OOCH_3).[22,23]

$$2CH_3OH \rightarrow HOCH_2CH_2OH + 2\dot{H} \quad (9)$$

Preferential formation of ethylene glycol may be driven in part by the stability of the hydroxymethyl radical ($\dot{C}H_2OH$), which is 40 kJ mol^{-1} more stable than the methoxy radical ($CH_3\dot{O}$) in the gas phase.[86,87] This is part of a trend toward the stabilization of carbon-centered radical sites relative to those on oxygen. The selective stabilization of hydroxymethyl, its barrierless recombination to yield ethylene glycol, and the abundance of both methanol and CO in observed interstellar ices point to widespread and abundant precursors of glyceraldehyde (**1**).

Conclusions

Observation of glyceraldehyde (**1**) intact and *in situ* during a space-simulation is a compelling demonstration of an abiotic route to sugar in the ISM that is replicable in the laboratory. Here, we provide compelling evidence on the formation of glyceraldehyde (**1**) in an ice composed of carbon monoxide, the second most abundant astrophysical ice component, as well as ethylene glycol, known to be abundant in the warm star-forming regions of aged interstellar molecular clouds.[21] These findings highlight the need for laboratory methods capable of probing the non-equilibrium solid-state chemistry, which governs the formation and evolution of complex organics in dense molecular clouds from which stars and planets originate. Astrophysical ices represent favorable environments for the production of increasingly complex organics.[16] The proposed route to glyceraldehyde (**1**), which proceeds through the synthesis of methanol and ethylene glycol, may represent a plausible path to a sugar in the ISM. The relative stabilization of carbon-centered radicals in comparison to oxygen-centered radicals, particularly in abundant methanol, has the potential to act as a mass-growth mechanism that guides astrochemistry toward the selective formation of increasingly long sugar alcohols, sugar acids, and sugars.

Production of glyceraldehyde (**1**) in dense molecular clouds represents a viable route towards a chemical feedstock necessary for the origins of life. The collapse of these clouds and the eventual formation of stars and planets implies that sugars were likely present in the material from which the Earth and solar system were formed. Bombardment by comets and icy meteorites—modern samples of which contain glyceraldehyde (**1**)[88]—during the late Hadean Eon (4 billion years ago) would further enrich the terrestrial surface with sugars and other complex organics during the era in which the surface of the planet stabilized and from which life originates.[3]

Author contributions

R. I. K. and R. C. F. designed research; J. H. M., J. W., & R. C. F performed research; J. H. M. analyzed data; J. H. M., J. W. and R. I. K. wrote the paper.

Conflicts of interest

The authors declare no competing interests.

Data availability

Essential data are provided in the main text and the supplementary information (SI). Supplementary information is available. See DOI: https://doi.org/10.1039/d5cp04397b.

Additional data are available from the corresponding author upon reasonable request.

Acknowledgements

The Hawaii group acknowledges support from the U.S. National Science Foundation (NSF), Division of Astronomical Sciences (AST-2403867). Computational investigation was supported by the U.S. National Science Foundation (NSF), Division of Astronomical Sciences (AST-2407815) and the Mississippi Center for Supercomputing Research.

References

1 E. R. R. Moody, S. Alvarez-Carretero, T. A. Mahendrarajah, J. W. Clark, H. C. Betts, N. Dombrowski, L. L. Szantho, R. A. Boyle, S. Daines, X. Chen, N. Lane, Z. Yang, G. A. Shields, G. J. Szollosi, A. Spang, D. Pisani, T. A. Williams, T. M. Lenton and P. C. J. Donoghue, *Nat. Ecol. Evol.*, 2024, **8**, 1654–1666.
2 J. W. Szostak, *Angew. Chem., Int. Ed.*, 2017, **56**, 11037–11043.
3 N. Kitadai and S. Maruyama, *Geosci. Front.*, 2018, **9**, 1117–1153.
4 J. M. Berg, J. L. Tymoczko and L. Stryer, *Biochemistry*, W. H. Freeman and Company, 7th edn, 2010.
5 C. T. Jurgenson, S. E. Ealick and T. P. Begley, *EcoSal Plus*, 2009, **3**, 1–16, DOI: 10.1128/ecosalplus.3.6.3.7.
6 M. A. Keller, G. Piedrafita and M. Ralser, *Curr. Opin. Biotechnol*, 2015, **34**, 153–161.
7 M. Ralser, *Biochem. J.*, 2018, **475**, 2577–2592.
8 M. Tessera, *Biol. Direct*, 2018, **13**, 18.
9 Y. A. Jeilani and M. T. Nguyen, *J. Phys. Chem. B*, 2020, **124**, 11324–11336.
10 F. Scossa and A. R. Fernie, *Comput. Struct. Biotechnol. J.*, 2020, **18**, 482–500.
11 P. L. Luisi, *Chem. Biodiversity*, 2012, **9**, 2635–2647.
12 P. L. Luisi, *Mol. Syst. Biol.*, 2014, **10**, 729.
13 M. Rivas, A. Becerra and A. Lazcano, *J. Mol. Evol.*, 2018, **86**, 27–46.
14 G. Cooper, N. Kimmich, W. Belisle, J. Sarinana, K. Brabham and L. Garrel, *Nature*, 2001, **414**, 879–883.
15 S. Pizzarello, D. L. Schrader, A. A. Monroe and D. S. Lauretta, *Proc. Natl. Acad. Sci. U. S. A.*, 2012, **109**, 11949–11954.
16 B. W. Carroll and D. A. Ostlie, *An Introduction to Modern Astrophysics*, Cambridge University Press, Cambridge, United Kingdom, 2nd edn, 2017.
17 R. W. Wilson, K. B. Jefferts and A. A. Penzias, *Astrophys. J.*, 1970, **161**, L43–L44.
18 P. Solomon, K. B. Jefferts, A. A. Penzias and R. W. Wilson, *Astrophys. J.*, 1971, **163**, L53–L56.
19 A. M. Smith and T. P. Stecher, *Astrophys. J.*, 1971, **164**, L43–L47.
20 J. A. Ball, C. A. Gottlieb, A. E. Lilley and H. E. Radford, *Astrophys. J.*, 1970, **162**, L203.
21 M. K. McClure, W. R. M. Rocha, K. M. Pontoppidan, N. Crouzet, L. E. U. Chu, E. Dartois, T. Lamberts, J. A. Noble, Y. J. Pendleton, G. Perotti, D. Qasim, M. G. Rachid, Z. L. Smith, F. Sun, T. L. Beck, A. C. A. Boogert, W. A. Brown, P. Caselli, S. B. Charnley, H. M. Cuppen, H. Dickinson, M. N. Drozdovskaya, E. Egami, J. Erkal, H. Fraser, R. T. Garrod, D. Harsono, S. Ioppolo, I. Jiménez-Serra, M. Jin, J. K. Jørgensen, L. E. Kristensen, D. C. Lis, M. R. S. McCoustra, B. A. McGuire, G. J. Melnick, K. I. Öberg, M. E. Palumbo, T. Shimonishi, J. A. Sturm, E. F. van Dishoeck and H. Linnartz, *Nat. Astron.*, 2023, **7**, 431–443.
22 C. Zhu, R. Frigge, A. Bergantini, R. C. Fortenberry and R. I. Kaiser, *Astrophys. J.*, 2019, **881**, 156.
23 S. Maity, R. I. Kaiser and B. M. Jones, *Phys. Chem. Chem. Phys.*, 2015, **17**, 3081–3114.
24 J. M. Hollis, F. J. Lovas, P. R. Jewell and L. H. Coudert, *Astrophys. J.*, 2002, **571**, L59–L62.
25 N. Brouillet, D. Despois, X. H. Lu, A. Baudry, J. Cernicharo, D. Bockelée-Morvan, J. Crovisier and N. Biver, *Astron. Astrophys.*, 2015, **576**, A129.
26 C. F. Chyba, P. J. Thomas, L. Brookshaw and C. Sagan, *Science*, 1990, **249**, 366–373.
27 C. R. Walton, J. K. Rigley, A. Lipp, R. Law, M. D. Suttle, M. Schönbächler, M. Wyatt and O. Shorttle, *Nat. Astron.*, 2024, **8**, 556–566.
28 C. Chyba and C. Sagan, *Nature*, 1992, **355**, 125–132.
29 J. OrÓ, *Nature*, 1961, **190**, 389–390.
30 D. Nesvorný, R. Li, A. N. Youdin, J. B. Simon and W. M. Grundy, *Nat. Astron.*, 2019, **3**, 808–812.
31 M. Pasek and D. Lauretta, *Origins Life Evol. Biospheres*, 2008, **38**, 5–21.
32 B. M. Jones and R. I. Kaiser, *J. Phys. Chem. Lett.*, 2013, **4**, 1965–1971.
33 M. J. Abplanalp, M. Förstel and R. I. Kaiser, *Chem. Phys. Lett.*, 2016, **644**, 79–98.
34 M. J. Abplanalp, S. Gozem, A. I. Krylov, C. N. Shingledecker, E. Herbst and R. I. Kaiser, *Proc. Natl. Acad. Sci. U. S. A.*, 2016, **113**, 7727–7732.
35 S. Maity, R. I. Kaiser and B. M. Jones, *Faraday Discuss.*, 2014, **168**, 485–516.
36 A. M. Turner, M. J. Abplanalp, S. Y. Chen, Y. T. Chen, A. H. H. Chang and R. I. Kaiser, *Phys. Chem. Chem. Phys.*, 2015, **17**, 27281–27291.
37 M. Bouilloud, N. Fray, Y. Bénilan, H. Cottin, M. C. Gazeau and A. Jolly, *Mon. Not. R. Astron. Soc.*, 2015, **451**, 2145–2160.
38 R. Kaiser and K. Roessler, *Astrophys. J.*, 1997, **475**, 144.
39 B. C. Ferrari, K. Slavicinska and C. J. Bennett, *Acc. Chem. Res.*, 2021, **54**, 1067–1079.
40 A. M. Turner and R. I. Kaiser, *Acc. Chem. Res.*, 2020, **53**, 2791–2805.
41 W. Yang, R. G. Parr and C. Lee, *Phys. Rev. A:At., Mol., Opt. Phys.*, 1986, **34**, 4586–4590.
42 A. D. Becke, *Phys. Rev. A:At., Mol., Opt. Phys.*, 1988, **38**, 3098–3100.
43 T. H. Dunning, *J. Chem. Phys.*, 1989, **90**, 1007–1023.
44 A. D. Becke, *J. Chem. Phys.*, 1993, **98**, 5648–5652.
45 M. J. Frisch, G. W. Trucks, H. B. Schlegel, G. E. Scuseria, M. A. Robb, J. R. Cheeseman, G. Scalmani, V. Barone, G. A. Petersson, H. Nakatsuji, X. Li, M. Caricato, A. V. Marenich, J. Bloino, B. G. Janesko, R. Gomperts, B. Mennucci, H. P. Hratchian, J. V. Ortiz, A. F. Izmaylov, J. L. Sonnenberg, D. Williams-Young, F. Ding, F. Lipparini, F. Egidi,

J. Goings, B. Peng, A. Petrone, T. Henderson, D. Ranasinghe, V. G. Zakrzewski, J. Gao, N. Rega, G. Zheng, W. Liang, M. Hada, M. Ehara, K. Toyota, R. Fukuda, J. Hasegawa, M. Ishida, T. Nakajima, Y. Honda, O. Kitao, H. Nakai, T. Vreven, K. Throssell, J. A. M. Jr., J. E. Peralta, F. Ogliaro, M. J. Bearpark, J. J. Heyd, E. N. Brothers, K. N. Kudin, V. N. Staroverov, T. A. Keith, R. Kobayashi, J. Normand, K. Raghavachari, A. P. Rendell, J. C. Burant, S. S. Iyengar, J. Tomasi, M. Cossi, J. M. Millam, M. Klene, C. Adamo, R. Cammi, J. W. Ochterski, R. L. Martin, K. Morokuma, O. Farkas, J. B. Foresman and D. J. Fox, *Gaussian 16, Revision A.03*, Gaussian, Inc., Wallingford CT, 2016.

46 K. Raghavachari, G. W. Trucks, J. A. Pople and M. Head-Gordon, *Chem. Phys. Lett.*, 1989, **157**, 479–483.

47 T. B. Adler, G. Knizia and H. J. Werner, *J. Chem. Phys.*, 2007, **127**, 221106.

48 K. A. Peterson, T. B. Adler and H. J. Werner, *J. Chem. Phys.*, 2008, **128**, 084102.

49 G. Knizia, T. B. Adler and H. J. Werner, *J. Chem. Phys.*, 2009, **130**, 054104.

50 H. J. Werner, P. J. Knowles, F. R. Manby, J. A. Black, K. Doll, A. Hesselmann, D. Kats, A. Kohn, T. Korona, D. A. Kreplin, Q. Ma, T. F. Miller, 3rd, A. Mitrushchenkov, K. A. Peterson, I. Polyak, G. Rauhut and M. Sibaev, *J. Chem. Phys.*, 2020, **152**, 144107.

51 C. Zhang, A. M. Turner, J. Wang, J. H. Marks, R. C. Fortenberry and R. I. Kaiser, *ChemPhysChem*, 2023, **24**, e202200660.

52 A. G. Yeghikyan, *Astrophys*, 2011, **54**, 87–99.

53 G. Socrates, *Infrared and Raman Characteristic Group Frequencies: Tables and Charts*, Wiley, Chichester, 2004.

54 K. Krishnan and R. S. Krishnan, *Proc. – Indian Acad. Sci., Sect. A*, 1966, **64**, 111–122.

55 J. Wang, A. M. Turner, J. H. Marks, R. C. Fortenberry and R. I. Kaiser, *ChemPhysChem*, 2024, **25**, e202400837.

56 A. Herath, M. McAnally, A. M. Turner, J. Wang, J. H. Marks, R. C. Fortenberry, J. C. Garcia-Alvarez, S. Gozem and R. I. Kaiser, *Nat. Commun.*, 2025, **16**, 5571.

57 J. Wang, C. Zhang, A. K. Eckhardt and R. I. Kaiser, *Chem. Sci.*, 2025, **16**, 21111–21120.

58 J. Wang, C. Zhang, A. Bergantini, O. V. Kuznetsov, M. M. Evseev, A. S. Shishova, I. O. Antonov and R. I. Kaiser, *J. Am. Chem. Soc.*, 2025, **147**, 29088–29097.

59 J. Wang, C. Zhang, J. H. Marks and R. I. Kaiser, *Astrophys. J.*, 2025, **984**, 138.

60 J. Wang, C. Zhang, J. H. Marks, M. M. Evseev, O. V. Kuznetsov, I. O. Antonov and R. I. Kaiser, *Nat. Commun.*, 2024, **15**, 10189.

61 J. Wang, J. H. Marks, E. A. Batrakova, S. O. Tuchin, I. O. Antonov and R. I. Kaiser, *Phys. Chem. Chem. Phys.*, 2024, **26**, 23654–23662.

62 J. Wang, J. H. Marks, R. C. Fortenberry and R. I. Kaiser, *Sci. Adv.*, 2024, **10**, eadl3236.

63 J. H. Marks, J. Wang, M. M. Evseev, O. V. Kuznetsov, I. O. Antonov and R. I. Kaiser, *Astrophys. J.*, 2023, **942**, 43.

64 J. Wang, J. H. Marks, A. M. Turner, A. A. Nikolayev, V. Azyazov, A. M. Mebel and R. I. Kaiser, *Phys. Chem. Chem. Phys.*, 2023, **25**, 936–953.

65 S. K. Singh, N. Fabian Kleimeier, A. K. Eckhardt and R. I. Kaiser, *Astrophys. J.*, 2022, **941**, 103.

66 N. F. Kleimeier and R. I. Kaiser, *J. Phys. Chem. Lett.*, 2022, **13**, 229–235.

67 J. Wang, A. A. Nikolayev, J. H. Marks, A. M. Turner, S. Chandra, N. F. Kleimeier, L. A. Young, A. M. Mebel and R. I. Kaiser, *J. Am. Chem. Soc.*, 2024, **146**, 28437–28447.

68 J. H. Marks, J. Wang, B.-J. Sun, M. McAnally, A. M. Turner, A. H. H. Chang and R. I. Kaiser, *ACS Cent. Sci.*, 2023, **9**, 2241–2250.

69 C. Zhang, J. Wang, A. M. Turner, J. H. Marks, S. Chandra, R. C. Fortenberry and R. I. Kaiser, *Astrophys. J.*, 2023, **952**, 132.

70 J. H. Marks, J. Wang, N. F. Kleimeier, A. M. Turner, A. K. Eckhardt and R. I. Kaiser, *Angew. Chem., Int. Ed.*, 2023, **62**, e202218645.

71 J. H. Marks, J. Wang, R. C. Fortenberry and R. I. Kaiser, *Proc. Natl. Acad. Sci. U. S. A.*, 2022, **119**, e2217329119.

72 J. Wang, A. M. Turner, J. H. Marks, C. Zhang, N. F. Kleimeier, A. Bergantini, S. K. Singh, R. C. Fortenberry and R. I. Kaiser, *Astrophys. J.*, 2024, **967**, 79.

73 A. M. Turner, A. S. Koutsogiannis, N. F. Kleimeier, A. Bergantini, C. Zhu, R. C. Fortenberry and R. I. Kaiser, *Astrophys. J.*, 2020, **896**, 88.

74 A. K. Eckhardt, A. Bergantini, S. K. Singh, P. R. Schreiner and R. I. Kaiser, *Angew. Chem., Int. Ed.*, 2019, **58**, 5663–5667.

75 C. Zhu, R. Frigge, A. Bergantini, R. C. Fortenberry and R. I. Kaiser, *Astrophys. J.*, 2019, **881**, 156.

76 A. Bergantini, P. Maksyutenko and R. I. Kaiser, *Astrophys. J.*, 2017, **841**, 96.

77 K. J. Chuang, G. Fedoseev, S. Ioppolo, E. F. van Dishoeck and H. Linnartz, *Mon. Not. R. Astron. Soc.*, 2016, **455**, 1702–1712.

78 G. W. Fuchs, H. M. Cuppen, S. Ioppolo, C. Romanzin, S. E. Bisschop, S. Andersson, E. F. van Dishoeck and H. Linnartz, *Astron. Astrophys.*, 2009, **505**, 629–639.

79 N. Watanabe and A. Kouchi, *Astrophys. J.*, 2002, **571**, L173–L176.

80 R. J. Morton and R. I. Kaiser, *Planet. Space Sci.*, 2003, **51**, 365–373.

81 R. I. Kaiser, G. Eich, A. Gabrysch and K. Roessler, *Astrophys. J.*, 1997, **484**, 487–498.

82 R. I. Kaiser and K. Roessler, *Astrophys. J.*, 1998, **503**, 959–975.

83 M. Conrad, *Ber. Dtsch. Chem. Ges.*, 2006, **43**, 3645–3664.

84 K. I. Öberg, *Chem. Rev.*, 2016, **116**, 9631–9663.

85 E. S. Wirström, W. D. Geppert, Å. Hjalmarson, C. M. Persson, J. H. Black, P. Bergman, T. J. Millar, M. Hamberg and E. Vigren, *Astron. Astrophys.*, 2011, **533**, A24.

86 T. L. Nguyen and J. F. Stanton, *J. Phys. Chem. A*, 2015, **119**, 7627–7636.

87 B. Ruscic and D. Bross, *Active Thermochemical Tables (ATcT) values based on ver. 1.130 of the Thermochemical Network*, Argonne National Laboratory, Lemont, Illinois, 2023, available at https://ATcT.anl.gov. (2023), DOI: 10.17038/CSE/1997229.

88 D. P. Glavin, A. S. Burton, J. E. Elsila, J. C. Aponte and J. P. Dworkin, *Chem. Rev.*, 2020, **120**, 4660–4689.

